forests

MDPI

Article

Combining UAV and Sentinel Satellite Data to Delineate Ecotones at Multiscale

Yuxin Ma [1], Zhangjian Xie [1], Xiaolin She [2], Hans J. De Boeck [1,3], Weihong Liu [1], Chaoying Yang [1,4], Ninglv Li [1], Bin Wang [1], Wenjun Liu [1,*] and Zhiming Zhang [1]

[1] School of Ecology and Environmental Sciences, Yunnan University, Kunming 650091, China; myx9837@gmail.com (Y.M.); zhangjianxie@mail.ynu.edu.cn (Z.X.); hans.deboeck@uantwerp.be (H.J.D.B.); liuweihong_ynu@stu.ynu.edu.cn (W.L.); yangchaoying@stu.ynu.edu.cn (C.Y.); lininglv@mail.ynu.edu.cn (N.L.); wb931022@hotmail.com (B.W.); zzming76@ynu.edu.cn (Z.Z.)
[2] Xinjiang Institute of Ecology and Geography, Chinese Academy of Sciences, Urumqi 830011, China; sehxiaolin@163.com
[3] Plants and Ecosystems (PLECO), Department of Biology, University of Antwerp, 2610 Wilrijk, Belgium
[4] CAS Key Laboratory of Tropical Forest Ecology, Xishuangbanna Tropical Botanical Garden, Chinese Academy of Sciences, Xishuangbanna 666303, China
* Correspondence: liuwj@ynu.edu.cn; Tel.: +86-150-0135-2217

Abstract: Ecotones, i.e., transition zones between habitats, are important landscape features, yet they are often ignored in landscape monitoring. This study addresses the challenge of delineating ecotones at multiple scales by integrating multisource remote sensing data, including ultra-high-resolution RGB images, LiDAR data from UAVs, and satellite data. We first developed a fine-resolution landcover map of three plots in Yunnan, China, with accurate delineation of ecotones using orthoimages and canopy height data derived from UAV-LiDAR. These maps were subsequently used as the training set for four machine learning models, from which the most effective model was selected as an upscaling model. The satellite data, encompassing Synthetic Aperture Radar (SAR; Sentinel-1), multispectral imagery (Sentinel-2), and topographic data, functioned as explanatory variables. The Random Forest model performed the best among the four models (kappa coefficient = 0.78), with the red band, shortwave infrared band, and vegetation red edge band as the most significant spectral variables. Using this RF model, we compared landscape patterns between 2017 and 2023 to test the model's ability to quantify ecotone dynamics. We found an increase in ecotone over this period that can be attributed to an expansion of 0.287 km^2 (1.1%). In sum, this study demonstrates the effectiveness of combining UAV and satellite data for precise, large-scale ecotone detection. This can enhance our understanding of the dynamic relationship between ecological processes and landscape pattern evolution.

Keywords: ecotone; unmanned aerial vehicles; canopy height model; machine learning; multisensory images; multiscale

Academic Editor: Saverio Francini

Received: 9 January 2025
Revised: 7 February 2025
Accepted: 24 February 2025
Published: 26 February 2025

Citation: Ma, Y.; Xie, Z.; She, X.; De Boeck, H.J.; Liu, W.; Yang, C.; Li, N.; Wang, B.; Liu, W.; Zhang, Z. Combining UAV and Sentinel Satellite Data to Delineate Ecotones at Multiscale. *Forests* **2025**, *16*, 422. https://doi.org/10.3390/f16030422

1. Introduction

Ecotones, first introduced by Clements [1] as transition zones between different habitats, are a basic unit in landscape studies. They are characterized by frequent material and energy flow [2] and support more species than adjacent ecosystems [3]. These zones are sensitive indicators of landscape ecology functions, patterns, and ecological processes, often signaling global climate changes [4,5]. In the context of forest fragmentation, which reduces patch sizes and increases forest edges [6], ecotones become more prevalent. Haddad et al. [7] estimated that 20% of forested land globally is situated within a 100-m-wide

ecotone, emphasizing their importance in fragmented landscapes. Due to their dynamic characteristics, ecotones are highly susceptible to impacts from climate change and anthropogenic activities [5,8]. Therefore, changes in environmental conditions can be inferred by monitoring changes in the location, width, and species composition of ecotones [9]. Ecotones can serve as buffer zones for protected areas to minimize the negative impact of anthropogenic activities on natural ecosystems [10].

Based on several studies on the structure, function, and edge effect of ecotones, a series of methods have been developed to quantitatively delineate ecotones, such as moving split window (MSW), landscape indices, remote sensing, and GIS methods [11–13]. Remote sensing technology facilitates large-scale mapping and monitoring of ecotones, utilizing data from Landsat, MODIS, Sentinel, or multi-source remote sensing data [8,14,15]. This technology has been used in detecting and analyzing ecotones such as forest-tundra [16], water-land [17], and agricultural-pastoral ecotones [18], where adjacent ecosystems typically exhibit clean, well-defined boundaries that can be easily detected from satellite imagery. However, challenges arise with forest-grassland ecotones inside forested areas, which are often small with blurred vegetation boundaries [19]. The spatial resolution of commonly used remote sensing satellites is mostly inadequate for detailed mapping of such fine-scale objects. This limitation often leads to these ecotones being ignored or simplified to lines in image classifications if they fall within a width of one or two pixels, and it is an oversimplification of realistic conditions [20,21]. To help resolve such issues and enable accurate mapping of ecotones at a fine scale, integrating satellite data with other spatial data sources is a promising way forward.

Unmanned Aerial Vehicles (UAVs) can provide ultra-high spatial resolution images of land cover, with pixel sizes on cm-level, making it possible to map smaller biotopes such as individual trees [22,23]. Beyond the high spatiotemporal resolution, UAVs can be used to acquire many of the same remotely sensed variables as those collected by manned airborne and spaceborne sensors. Three-dimensional data from Airborne Laser Scanning (ALS) allow accurate determination of vegetation height, and this capability has been utilized to describe vegetation structure within the ecotones [24,25]. Furthermore, ALS data have been integrated with multispectral satellite imagery to map ecotones over large areas [24]. Despite limited spatial and temporal coverage, UAV data can overcome spatiotemporal mismatches between field and remote sensing data [26,27]. The data collected by UAVs can serve as an alternative source for reference data collection, effectively bridging the gap between regional remote sensing monitoring and quadrat survey data. Moreover, integrating UAV data with freely available satellite imagery allows for the creation of cost-effective, large-scale maps, enhancing the accessibility and utility of remote sensing for natural resource management and monitoring.

In this study, we put forward a methodological framework to delineate forest-grassland ecotones across large areas, using multi-source remote sensing data conducted at the Ailao Mountain National Nature Reserve (Yunnan, China). The main objectives are to: (a) Successfully detect ecotones to achieve more accurate land-cover maps by combining orthoimages and LiDAR data from UAVs; (b) build an ecotone upscaling model based on machine learning algorithms using the backscattering coefficient of Sentinel-1, multispectral bands and spectral vegetation index from Sentinel-2, and combining these with topographic variables; and (c) apply this ecotone upscaling model on satellite images of different years to monitor dynamic changes of ecotones across 6 years and evaluate landscape fragmentation using landscape metrics.

2. Materials and Methods

2.1. Overview of the Analyses

The workflow of this study (Figure 1) can be summarized into five main stages: (i) acquisition of UAV data; (ii) pre-processing of UAV orthophotos and LiDAR data to generate the visible light images and the canopy height model along with derived products; (iii) classification of the imagery to create fine-scale ecotone map; (iv) construction of ecotone upscaling model based on machine learning algorithms; and (v) spatiotemporal dynamic analysis incorporating detection of ecotones at large scale in different periods and landscape fragmentation assessment using landscape metrics.

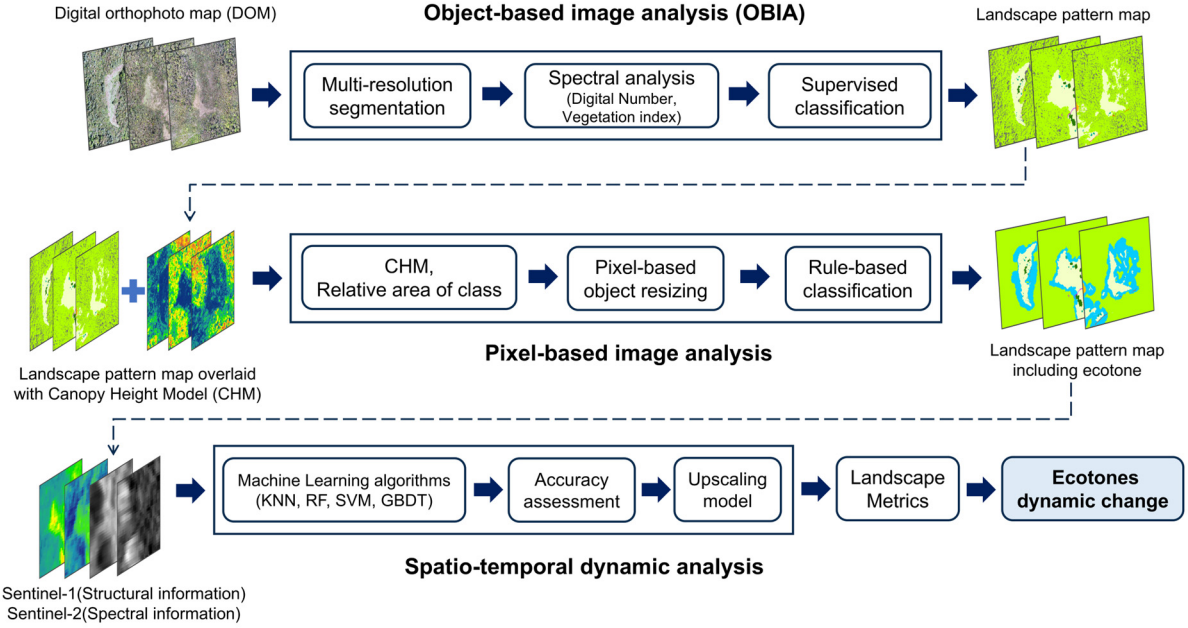

Figure 1. Workflow of the proposed upscaling model for ecotone detection at landscape scale. KNN, RF, SVM, and GBDT represent four machine learning algorithms: k-nearest-neighbors, random forest, support vector machine, and gradient boosting decision tree.

2.2. Study Area

This study was conducted in the Ailao Mountain area in central Yunnan Province, China. The region is at the crossroads of three important natural geographic zones, namely the Yunnan-Guizhou Plateau, the Hengduan Mountains, and the Qinghai-Tibet Plateau, where a diverse range of biota converge from east to west and north to south, resulting in high biodiversity and making it a very relevant zone for ecological research [28]. Within this biodiversity hotspot, the specific study area (Figure 2) is located in the Xujiaba area (24°32′ N, 101°01′ E) in the Ailao Mountain National Nature Reserve, with an altitude of 2400–2600 m [29]. The study area belongs to the southwest monsoon region, with distinct dry (November to April) and rainy seasons (May to October), the average annual temperature in this area is 11.3 °C, and the average annual precipitation is 1931 mm. The reserve is characterized by large areas of continuous subtropical broad-leaved evergreen forests, and the tree layer is dominated by *Lithocarpus hancei*, *Lithocarpus xylocarpus*, *Schima noronhae*, *Hartia sinensis*, *Camellia forrestii*, *Manglietia insignis*, *Michelia floribunda*, etc. [30]. In this study, three types of forest-grassland ecotones, named Bojiba (BJB), Dujuanba (DJB), and Shengtaizhan (STZ) were investigated, each with an area of 0.16 km^2 and a total area of 0.48 km^2. These plots represent post-cultivation, naturally formed, and cultivation-influenced ecotones, respectively. Each plot features a central grassland area encircled by

forests, which simplifies feature identification from UAV orthophotos and satellite data, especially in mountainous areas with complex terrain.

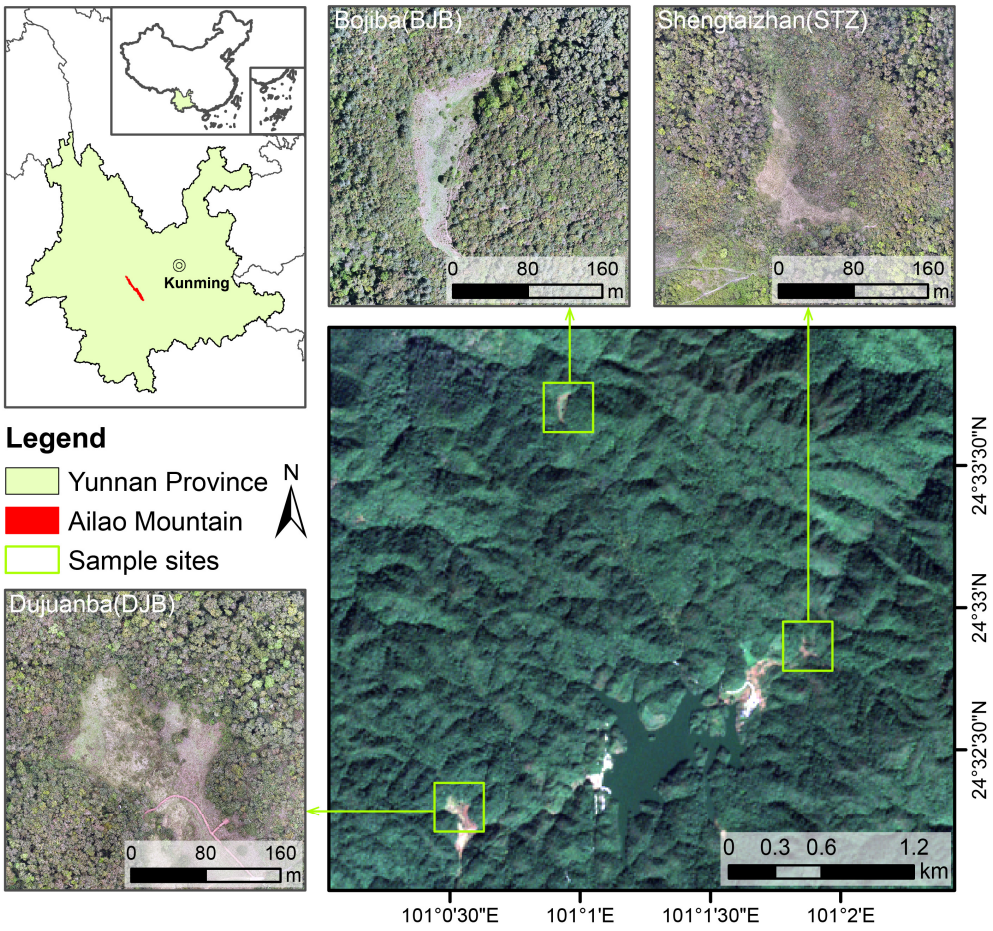

Figure 2. The location of the study area and the distribution of three sample sites.

2.3. Data Acquisition

2.3.1. UAV Data Acquisition and Processing

Visible light images and airborne LiDAR data for three sample plots were collected on 20–25 April 2022, using the DJI Phantom 4 Pro RTK (DJI, Shenzhen, China) and DJI M600Pro UAS platform, respectively. The survey was conducted in late April to make use of stable weather conditions, ensuring high-quality remote sensing data and precise ecotone delineation. Since the sample sites were located in a steep mountainous area with large terrain undulations, a ground imitation flight methodology adjusting the flight height according to terrain changes was used to collect UAV data to ensure flight safety and result quality. The first step of the aerial survey was to collect the initial Digital Surface Model (DSM) using the DJI Phantom 4 Pro RTK, where the flight altitude was set to the highest altitude of the sample site plus 150 m. Subsequently, the flight altitude was set to exceed the initial DSM by 70 m for a ground imitation flight. In all aerial surveys, the longitudinal and lateral overlap of the flight strips exceeded 85%.

After UAS data collection, three high-resolution (0.04 m/pix) orthoimages of each sample site were generated using the Agisoft Metashape 1.7.6 (https://www.agisoft.com, accessed on 19 May 2023) following the orthoimage generation process flow. The collected UAV lidar data of each study site were first imported into the LiAcquire 4.0 (GreenValley International Inc., Beijing, China) for pre-processing and then processed following the same protocol, including denoising, filtering, and normalization using the LiDAR360 5.2 (GreenValley International

Inc., Beijing, China). Based on the normalized lidar point clouds, the Digital Surface Model (DSM), Digital Terrain Model (DTM), and Canopy Height Model (CHM = DSM − DTM) were calculated at a spatial resolution of 0.5 m using ArcGIS Pro 2.8.3.

2.3.2. Satellite Image Acquisition

Satellite images covering the study area, including Sentinel-2 (S2) and Sentinel-1 (S1), were acquired and processed through Google Earth Engine (GEE, https://code.earthengine.google.com/, accessed on 10 March 2024). To reduce the impact of clouds, all available imageries of S2A and S1 with cloud cover less than 5% from March to May 2022 were collected. S2 images cover 13 spectral bands from visible and near-infrared to short-wave infrared with a revisit period of 5 days and a spatial resolution from 10 to 60 m. S2 images were downloaded from the COPERNICUS/S2_SR collection. Since the width of the ecotone is limited, we only selected the 10 m and 20 m resolution bands in the S2 images and resampled the 20 m resolution band to 10 m using bilinear interpolation to facilitate integration and consistency. We obtained the reflectance of 10 raw bands and used the median-value composite method to generate 13 vegetation indices based on these 10 raw bands.

S1 consists of two C-band polar-orbiting satellites, Sentinel-1A and Sentinel-1B, carrying synthetic aperture radar (SAR) that provides continuous imagery across day and night in all weather conditions. Sentinel-1 supports both single-polarization mode (HH or VV) and dual-polarization mode (HH + HV or VV + VH). VV and VH are commonly used for the estimation of vertical parameters. S1 images with VV and VH polarization were downloaded from the Copernicus S1_GRD collections (IW instrument mode). Two indices were also calculated from the backscattering coefficients [31,32].

$$sum = VV + VH \quad (1)$$

$$ratio = VV / VH \quad (2)$$

where *sum* and *ratio* indicate the sum and ratio of backscattering coefficients, respectively. VV denotes single co-polarization, vertical transmit/horizontal receive, while VH represents dual-band cross-polarization, vertical transmit/horizontal receive.

Topography factors were obtained from digital elevation model (DEM) data with 12.5 m spatial resolution, downloaded from ALOS-PALSAR data at https://search.asf.alaska.edu/ (accessed on 20 March 2024). To match the resolution of S1 and S2 images, we also resampled the elevation data to 10 m resolution and calculated the slope for each pixel based on it.

There are 29 variables extracted from satellite images, as detailed in Table 1, which include 10 S2 spectral features, 13 vegetation indices, 4 S1 structural features, and 2 topography factors. These variables will be referred to below as the 29 variables. We generated a 10 m × 10 m fishnet and label points in ArcGIS 10.7 to align with the resolution of these variables and utilized the R package "terra" (version 1.7-55) [33] to extract variable values at corresponding fishnet points.

Table 1. Features from remote sensing data as inputs of machine learning models for ecotone upscaling.

Type	Name	Equation or Description	Source
Spectral band	Blue	Central wavelength: 490 nm	Sentinel-2
	Green	Central wavelength: 560 nm	Sentinel-2
	Red	Central wavelength: 665 nm	Sentinel-2
	Red Edge 1	Central wavelength: 705 nm	Sentinel-2
	Red Edge 2	Central wavelength: 740 nm	Sentinel-2

Table 1. *Cont.*

Type	Name	Equation or Description	Source
	Red Edge 3	Central wavelength: 783 nm	Sentinel-2
	NIR 1	Central wavelength: 842 nm	Sentinel-2
	NIR 2	Central wavelength: 865 nm	Sentinel-2
	SWIR 1	Central wavelength: 1610 nm	Sentinel-2
	SWIR 2	Central wavelength: 2190 nm	Sentinel-2
C-band SAR	VV	Single co-polarization, vertical transmit/horizontal receive	Sentinel-1
	VH	Dual-band cross-polarization, vertical transmit/horizontal receive	Sentinel-1
	VV + VH	The sum of backscattering coefficients	Sentinel-1
	VV / VH	The ratio of backscattering coefficients	Sentinel-1
Topography factor	Elevation	The vertical distance above sea level	ALOS
	Slope	The ratio of the vertical height to the horizontal distance	ALOS
Vegetation Index	EVI	2.5 × (NIR − Red) / (NIR + 6 × Red − 7.5 × Blue + 1)	Sentinel-2
	GNDVI	(NIR 1 − Green) / (NIR 1 + Green)	Sentinel-2
	IRECI	(Red Edge 3 − Red) / (Red Edge 1/Red Edge 2)	Sentinel-2
	MSI	SWIR 1 / NIR 2	Sentinel-2
	MSR	(NIR 1 / Red − 1) / (sqrt (NIR 1 / Red + 1.0))	Sentinel-2
	NBR	(Red Edge 2 − SWIR 2) / (Red Edge 2 + SWIR 2)	Sentinel-2
	NDVI	(NIR 1 − Red) / (NIR 1 + Red)	Sentinel-2
	RENDVI	(Red Edge 3 − Red) / (Red Edge 3 + Red)	Sentinel-2
	RRI1	NIR 2 / Red Edge 1	Sentinel-2
	SLAVI	NIR 2 / (Red Edge 1 + SWIR 2)	Sentinel-2
	SR	NIR / Red	Sentinel-2
	SRRE	Red Edge 1 / Red	Sentinel-2
	VIg	(Green − Red) / (Green + Red)	Sentinel-2

NIR—Near Infrared; SWIR—Short Wave Infrared.

2.4. Methods

2.4.1. Extraction and Classification of Ecotones at Fine Scale

The ecotones between forest and grassland refer to mixed vegetation above the grass layer but below the overstory formed by a combination of side branches of canopy trees, small trees, and shrubs [1]. Based on this, variations in height served as indicators of the environmental gradient along the forest-grassland boundary [23,34]. The first step to extract ecotones between forest and grassland is mapping the land-cover map for three sample plots. In our case, we chose object-based image classification (OBIC) in the eCognition developer 10.3 to distinguish forest, grass, shadow, and other classes (farmland, road, etc.) based on UAV orthoimages. Then, we adopted the method developed by Hou and Walz [34], which can be concluded as a "shrinking process" to detect the ecotones. There were two prerequisites used for extracting the ecotones: vegetation height and proportion of non-ecotone pixels. By overlaying the land-cover map with the Canopy Height Model (DSM-DTM), the average height of forest (H_f) and grassland (H_g) in each sample site was

calculated using the "zonal statistics" tool in ArcGIS 10.7. In addition to the height limits, the proportion of non-ecotone pixels within the moving window was set to less than 60% based on the model from Riitters et al. [35]. To minimize the impact of shadows, this class was reclassified to forest or grassland based on the proportion of classes in the nearest pixel before running the shrinking procedure. The shrinking process was completed in eCognition developer 10.3 using the "pixel-base object resizing" tool. A window moving along the edge between forest and grassland was used to judge pixels under two conditions (height restriction and area ratio), the specific processes (Figure 3) were (1) shrink forest along the border pixels where CHM < H_f and the proportion of forest pixels within a moving window (201 by 201 pixels, which is c. 0.01 km^2) < 60% and (2) shrink grassland along the border pixels where CHM > H_g and the proportion of grassland pixels within a moving window (201 by 201 pixels) < 60%. Finally, impurities inside the ecotones were eliminated by removing forest/grassland pixels smaller than four pixels and enclosing by ecotones to avoid some mixed pixels. Following the processing sequence described above, we produced ecotone-containing land-cover maps to serve as training examples for the subsequent ecotone-upscaling models.

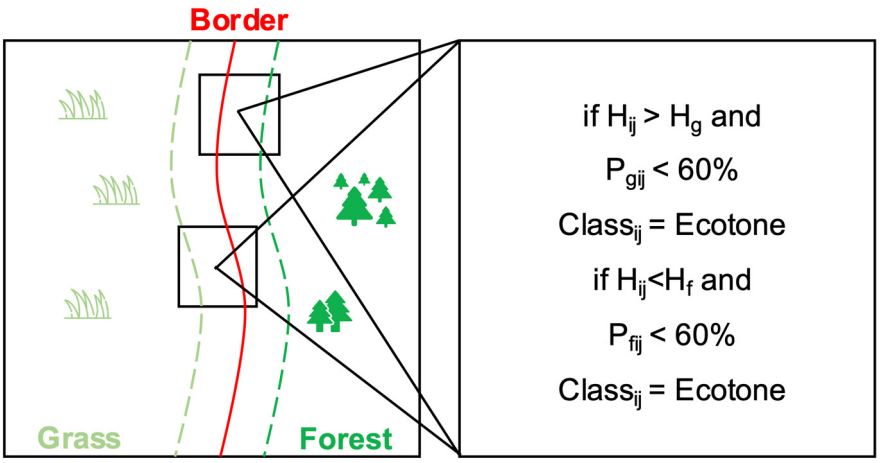

Figure 3. Shrinking process diagram. H_{ij} represents the CHM of any pixel, H_f represents the average height of the forest, and H_g represents the average height of the grassland. P_{gij} represents the proportion of grass pixels within a moving window. P_{fij} represents the proportion of forest pixels within a moving window.

2.4.2. Quantifying the Landscape Pattern Containing Ecotones

Compared with traditional ecotone detection methods, spatially continuous detection offers a significant advantage by enabling the quantification of ecotones. To assess the landscape characteristics of ecotones, a series of landscape metrics at the class level were computed using the "landscapemetrics" package [36] in R 4.2.3, including total area (TA), percentage of landscape (PLAND), total edge (TE), shape index (SI), and edge contrast index (ECON). These metrics facilitate a quantitative assessment of ecotone characteristics and the effects of their inclusion or exclusion on landscape patterns.

Total Area quantifies the size of landscape classes and their composition, providing a direct assessment of the scale of various landscape elements. The vegetated area significantly influences the number of species it can harbor due to the area effect [37]. The percentage of the landscape is used to quantify the landscape weight of each class in the landscape, serving as an indicator of landscape composition. The value of PLAND indirectly reflects the contribution of the landscape of each class to the spatial heterogeneity within the landscape [38]. The total edge reflects the total edge length of a class, with longer edge lengths generally associated with larger edge effects, which could influence ecological

processes along class boundaries. The shape index is used to assess the geometric complexity of landscape elements, with more complex shapes potentially reflecting more frequent disturbances. Furthermore, TE and SI are employed to determine the edge characteristics of land cover types, which can be related to the edge effect of the corresponding land cover class [39]. Finally, ECON is used to describe the relative difference between adjacent classes. High contrast values indicate significant differences, suggesting the transitions between them are narrow or absent [34].

2.4.3. Ecotones Upscaling Model

In this study, we used the machine learning algorithm from the scikit-learn library (version 1.2.2) in Python 3.10.9 to construct the ecotone upscaling model, combining the results of the ecotones extracted based on UAV data with 29 variables extracted from satellite images. The term "upscaling" here refers to utilizing high-resolution UAV data to enhance the classification accuracy and interpretative capability of satellite imagery across large areas.

Four different machine learning algorithms were tested to construct the model: k-nearest-neighbors (KNN), random forest (RF), support vector machine (SVM), and gradient boosting decision tree (GBDT). Since the model parameters affected the performance of Machine Learning (ML) algorithms, the grid search method was used in this study to find the optimal parameter values that would result in the highest average accuracy for each ML algorithm (Table 2).

Table 2. Results of the hyper-parameter optimization process.

Model	Optimal Parameter Values
K nearest neighbor	n_neighbors—10, metric—manhattan, weights—distance
Random forest	n_estimators—100, max_depth—13, max_features—sqrt
Support vector machine	penalty value C—1.0, kernel functions—linear
Gradient boost decision tree	n_estimators—450, learning_rate—0.1, max_depth—7

K-nearest-neighbors is a non-parameter algorithm that uses an instance-based learning approach, or "lazy learning". Unlike other classifiers that generate a predictive model, k-NN directly compares each unknown sample with the training data [40,41], assigning it to the most common class among the k-nearest training samples in the feature space. Therefore, K is the key tuning parameter in this classifier, which largely determines the performance of the KNN classifier.

The random forest classifier is a decision-tree-based ensemble classifier, which operates by constructing a number of decision trees in the training process and outputting the prediction classes. RF has become popular within the remote sensing community due to its high predictive accuracy for high-dimensional data and low sensitivity to overfitting, multicollinearity, and outliers [42].

Support vector machine is a non-parametric supervised machine learning algorithm initially described by Cortes and Vapnik [43], based on the concept of structural risk minimization (SRM). This model seeks the optimal separating hyperplane that maximizes the distance between the nearest samples (support vectors) to the plane and effectively separates classes [44–46]. The method is suitable for small-sample, nonlinear prediction problems and has good generalization ability [47].

Gradient boosted decision trees classifier is a boosting ensemble machine learning method that combines multiple decision trees [48]. The GBDT implements a classification task by building an ensemble of weak prediction models, typically decision trees, to create

a strong prediction model. It improves the accuracy of classification through multiple iterations, each of which reduces the residuals of the previous iteration and continuously adjusts the weights of misclassified samples. GBDT can fit the true distribution of data and has a strong generalization ability.

The 29 variables (for details, see Table 1) were imported into these models to detect ecotones at a large scale. To define the best set of features for detecting ecotones, these data were divided into three subsets: (1) "s1", which considers only the backscattering coefficients for the S1 data and the indices calculated from the original data of S1 data; (2) "s2", which considers only the multispectral bands from the S2 data and the vegetation indices calculated from these reflectance bands; and (3) "all", which include all features from S1 and S2 data. The topographic features were included in all three subsets. Based on the three subsets of variables, 70% of pixels in the landcover map of ecotones were randomly selected as training samples, and the remaining 30% of data were selected as the verification samples to evaluate the classification accuracy.

To evaluate the land cover classification accuracy, the accuracy metrics, including the overall accuracy (OA) and kappa coefficient (k), have been widely used [49]. Overall accuracy was determined as the ratio of correctly classified samples to the total number of samples. The kappa coefficient was a measurement to test whether the predicted results of the model were consistent with the actual classification results [50].

By comparing the OA and k of different models, we selected the most effective model as an upscaling model. The mean decrease accuracy which refers to how much the prediction accuracy of the model was reduced after deleting this feature was used to determine the significance of each feature. We subsequently identified the features suitable for ecotone detection, thus obtaining a large-scale landscape pattern map. All modeling steps were developed in the Python environment, using scikit-learn [51].

2.4.4. Spatio-Temporal Dynamic Analysis of Ecotones

We employed the overlapping region of Ailao Mountain National Nature Reserve and one scene Sentinel-2 image as the area for spatio-temporal dynamic analysis using the upscaling model. The selection of the temporal range, spanning from 2017 to 2023, was based on image acquisition timing, quality, and data availability. Although the Sentinel-2 satellite was launched in 2015 [52], data for our area before 2017 was limited and often cloud-covered, while 2023 is the most recent year with a full dataset. The 2017–2023 range thus provides the most extensive and reliable imagery series available for our study area. Sentinel-1 and Sentinel-2 datasets for this period were downloaded from the GEE platform, and the 29 features mentioned in Table 1 were obtained after preprocessing. Subsequently, these features were processed through the upscaling model to generate large-scale maps of ecotones. Due to the limited resolution of satellite imagery, fine-scale features like single trees could not be effectively identified, unlike with higher-resolution UAV data. To ensure methodological consistency across various data sources, we therefore classified non-forest and non-ecotone areas collectively as "Others".

To assess landscape fragmentation, we focused on the edge effect, isolation effect, and patch size effect, which are deemed the most important features for understanding landscape fragmentation [7]. These effects were quantified using three landscape pattern metrics, including edge density (ED), patch density (PD) and mean patch area (MPA), respectively. The three landscape metrics were calculated at the class level using the "landscapemetrics" package [36] in R 4.2.3 based on the large-scale maps of ecotones described above. A synthesized fragmentation index (FI) [53] was constructed using the mean values of ED, PD, and MPA in the ArcGIS 10.7, providing a synthetic measure of landscape fragmentation.

3. Results

3.1. Ecotone Detection at Fine Scale

The canopy height of each sample site was extracted from the normalized lidar point clouds. Figure 4 shows the DTM, DSM, and CHM of each site. From the results, the vegetation height changed obviously at the boundary between forest and grassland.

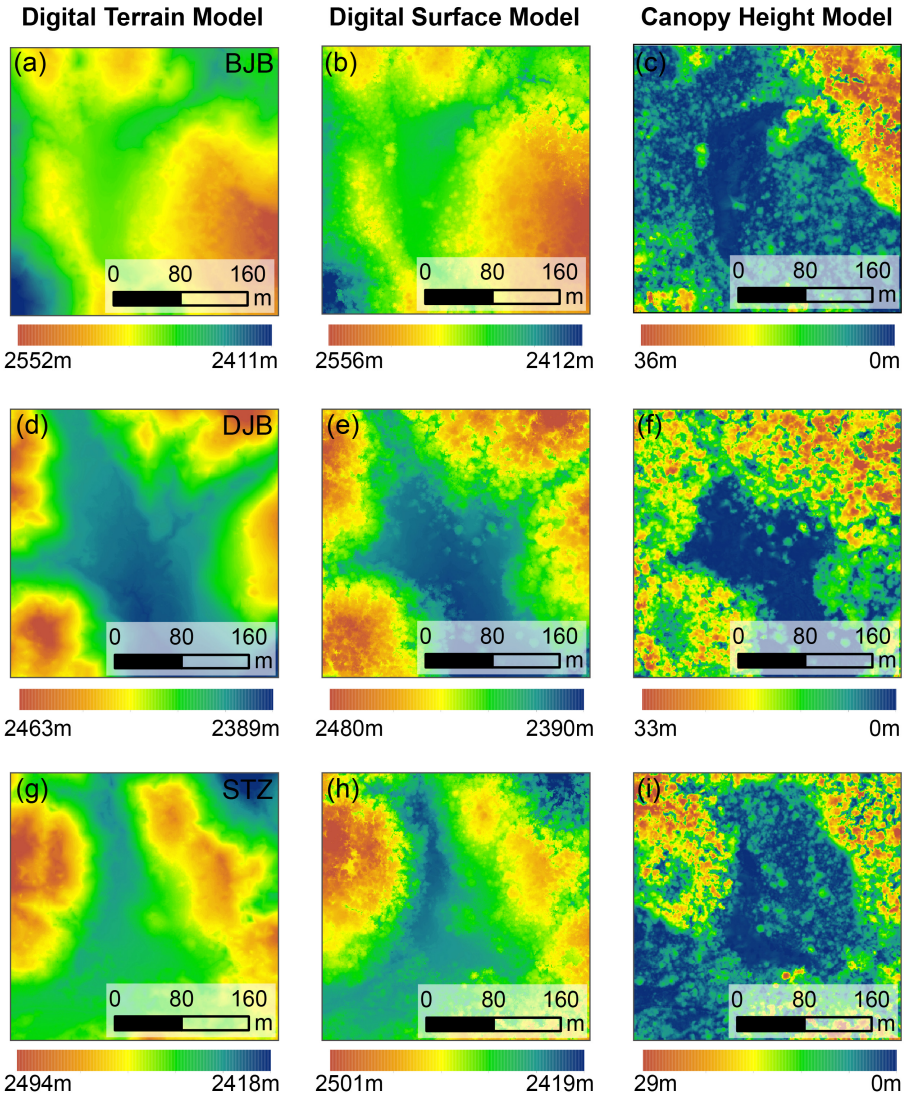

Figure 4. The digital terrain model (DTM), digital surface model (DSM), and canopy height model (CHM) of the three sample sites used in our study (for details, see Figure 2). (**a**–**c**) show the BJB site, (**d**–**f**) show the DJB site, and (**g**–**i**) show the STZ site.

Based on the high-resolution orthoimages of UAV and CHM derived from LiDAR data and following the classification framework proposed in Section 2.4.1, a fine-scale landscape pattern map was obtained (Figure 5d–f), which is an essential prerequisite for accurate detection of ecotones. Based on the classification results (Figure 5d–f), we calculated the average height of forest and grassland classes for each sample site. The average height of the forest class in the three sample sites BJB, DJB, and STZ was 8.20 m, 12.24 m, and 7.65 m, and the average height of the grassland class was 0.87 m, 0.99 m, and 0.84 m, respectively.

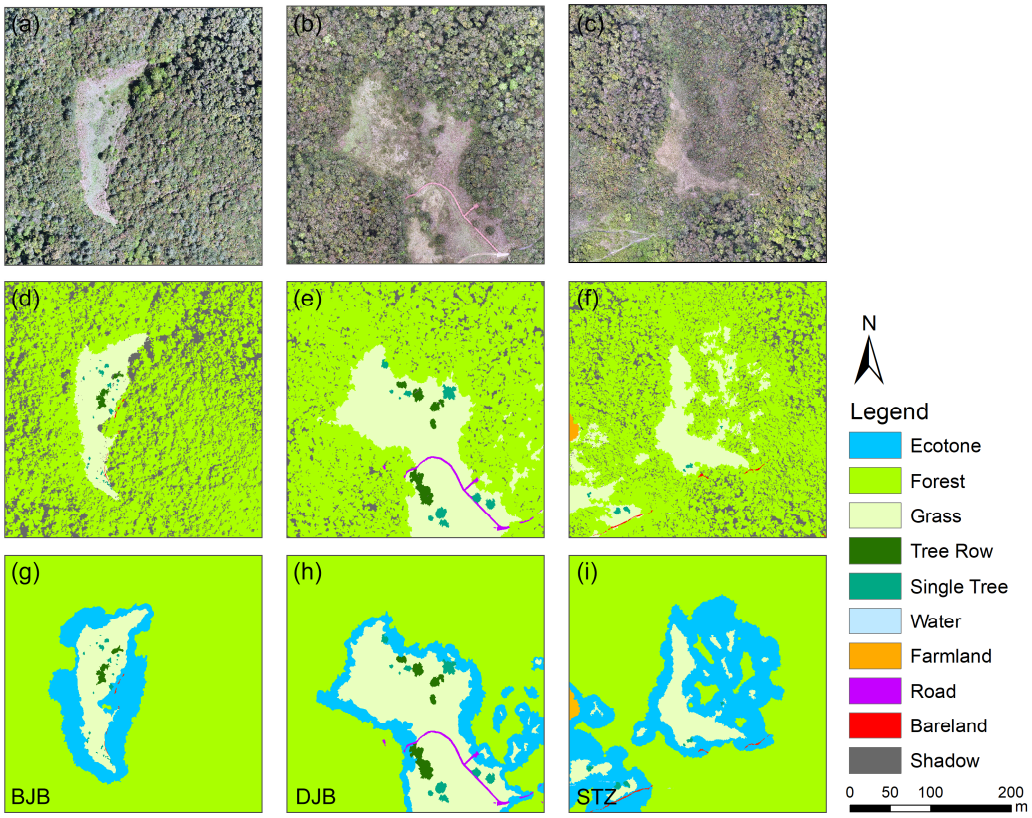

Figure 5. The orthoimage of three sample plots (**a**–**c**), fine-scale landscape pattern map derived from UAV-data (**d**–**f**), and landscape pattern maps including the delineated ecotones (shadows removed) (**g**–**i**).

The landscape pattern maps, including ecotones, were obtained using the object-based image analysis (Figure 5g–i) and the size of ecotones was calculated based on these maps (Table 3). This revealed the influence of land management practices on ecological processes. The STZ site, still under active farming, presented the largest ecotone area due to more human interventions. In contrast, DJB represents a transition zone in a more natural state, while BJB, in a phase of restoration after farming abandonment, showed the smallest ecotone area. In areas with complex terrain like our study area, UAV-derived orthoimages often display shadows caused by the terrain or large structures such as trees. To ensure the accuracy of ground features, we mark "shadow" as a separate class. This classification enhances the accuracy of the analysis and interpretation of actual ground conditions, ensuring data quality and improving the reliability of research findings.

Table 3. Area and proportion of ecotones.

Plots	Area (km^2)	Proportion (%) [1]
BJB	0.0113	11
DJB	0.0123	12.06
STZ	0.0253	24.72

[1] The "Proportion (%)" indicates the area percentage of each plot classified as ecotone, with each plot covering an area of 0.1024 km^2.

According to Forman [54], the ecotones in this region can be mainly detected in two forms: (1) the thin transitions along the forest/field border and (2) wide forest borders with convex or concave shapes. The ecotones at BJB are simpler, consisting solely of the thin transition type along the forest–grassland junction. Conversely, DJB and STZ exhibit both

forms of ecotones, indicating a more complex interaction between forest and adjacent land at these sites.

From the quantitative results (Table 4), when ecotones were incorporated into the analysis (compared to the classification excluding ecotones), the value of each landscape metric decreased, and the ecotones had the maximum boundary length. Specifically, the ECON values decreased upon considering ecotones. Taking BJB as an example, the ECON values for the forest class decreased from 22.4 (without ecotones) to 18.9 (with ecotones), indicating a reduction in the average contrast of forests due to the presence of ecotones. This trend was consistent across other land cover classes, leading to a smoother transition between grassland and forest.

Table 4. A series of common landscape metrics used to quantify some elements of the landscape.

Plot	Class	TA (hm^2)	PLAND (%)	TE (m)	SI	ECON
BJB	Ecotone	-/1.13 [1]	-/11.00	-/2.01	-/4.73	-/26.24
	Forest	9.40/8.34	91.83/81.45	0.99/1.10	1.85/1.75	22.38/18.87
	Grass	0.78/0.72	7.65/7.04	1.53/1.32	4.3/3.88	45.43/30.82
DJB	Ecotone	-/1.23	-/12.05	-/3.84	-/2.84	-/26.54
	Forest	7.72/6.65	75.35/64.94	2.24/2.07	3.06/2.01	46.48/16.96
	Grass	2.27/2.11	22.19/20.56	3.44/2.84	1.7/1.89	68.99/26.00
STZ	Ecotone	-/2.53	-/24.73	-/5.02	-/2.19	-/25.43
	Forest	8.97/6.94	87.65/67.77	5.21/2.57	1.31/1.55	49.61/27.08
	Grass	1.20/0.70	11.76/6.81	5.28/1.97	1.77/1.85	48.73/25.4

[1] The values before "/" were calculated without considering ecotones; values after "/" include ecotones.

3.2. Detection of Ecotones at Large Scale

Among the three subsets of input variables, the "all" subset could obtain the highest detection accuracy of ecotones. Combining Sentinel-1 with Sentinel-2 data can slightly improve accuracy. The results indicated that the Random Forest (RF) model outperformed the other three models in this study (Table 5). Therefore, RF was chosen as an upscaling model and the combination of S1 and S2 features were chosen as input variables for upscaling the ecotones from fine (UAV) to large (Satellite) scale.

Table 5. The performance of various feature subsets for the detection of ecotones using four ML algorithms.

Algorithm	Features Subset	OA	Kappa	Precision	Recall	F1-Score	Training Time (s) [1]
RF	s1	0.79	0.48	0.69	0.62	0.67	311
	s2	0.88	0.73	0.83	0.77	0.82	314
	all	0.90	0.78	0.86	0.84	0.85	455
SVM	s1	0.77	0.35	0.64	0.52	0.51	493
	s2	0.87	0.71	0.83	0.76	0.79	508
	all	0.89	0.76	0.85	0.82	0.84	505
KNN	s1	0.77	0.42	0.64	0.58	0.59	513
	s2	0.87	0.72	0.83	0.77	0.80	519
	all	0.88	0.74	0.84	0.80	0.82	533
GBDT	s1	0.80	0.52	0.71	0.64	0.63	452
	s2	0.88	0.76	0.84	0.80	0.80	482
	all	0.89	0.77	0.85	0.82	0.83	714

[1] The "Training time" data were obtained using a MacBook Pro equipped with an M1 Pro chip.

We compared the land cover classification results for three sample plots using the upscaling model versus only satellite imagery (Figure 6). The data used for comparison were the UAV data collected in 2022 and the satellite imagery from the same year. The upscaling model outperformed satellite-only imagery, achieving an ecotone classification accuracy of 0.9 compared to 0.25. This highlights the importance of combining UAV data with satellite imagery for delineating ecotones across large areas.

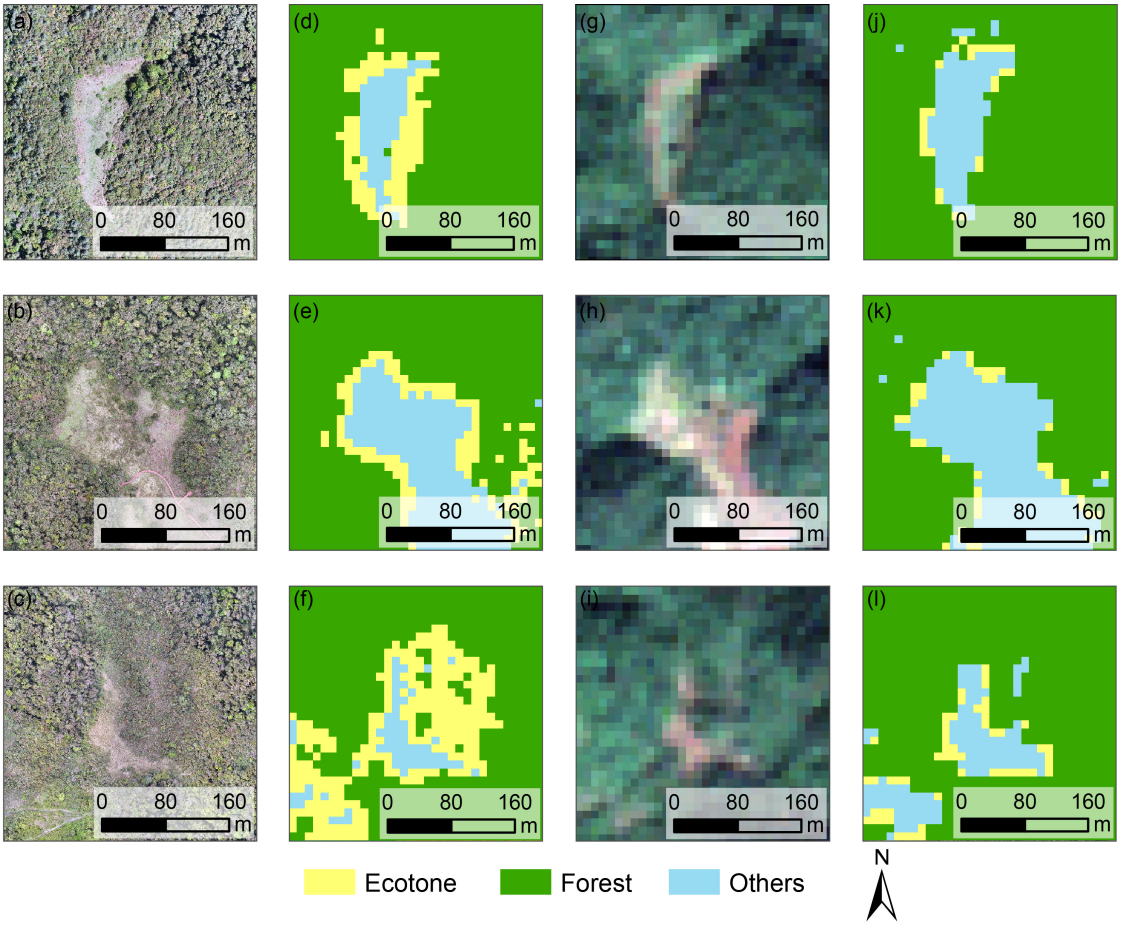

Figure 6. Comparison of the classification using only satellite data and the upscaling model. The orthoimage of three sample plots (**a**–**c**), landscape pattern map derived from the upscaling model (**d**–**f**), Sentinel-2 imagery of three sample plots (**g**–**i**), and landscape pattern map derived from only satellite data (**j**–**l**).

We also calculated the precision of all four algorithms for each class (Table 6). Ecotones had the lowest precision, which highlights the difficulties in distinguishing this class from the rest. The RF method performed better than other methods.

Table 6. Detection precision of three classifications.

Algorithm	Ecotone	Forest	Others
RF	0.78	0.94	0.89
SVM	0.76	0.92	0.88
KNN	0.72	0.92	0.87
GBDT	0.77	0.93	0.83

Subsequently, the importance of input variables for RF was calculated (Figure 7). As indicated by the variable importance for detecting ecotones, multispectral data from

Sentinel-2 were far more suitable than the SAR data from Sentinel-1. In these bands, the red band (band 4), shortwave infrared band (band 12), and vegetation red edge band (band 5) were identified as the three most important variables. VIg was the most important vegetation index for the ecotone upscaling model.

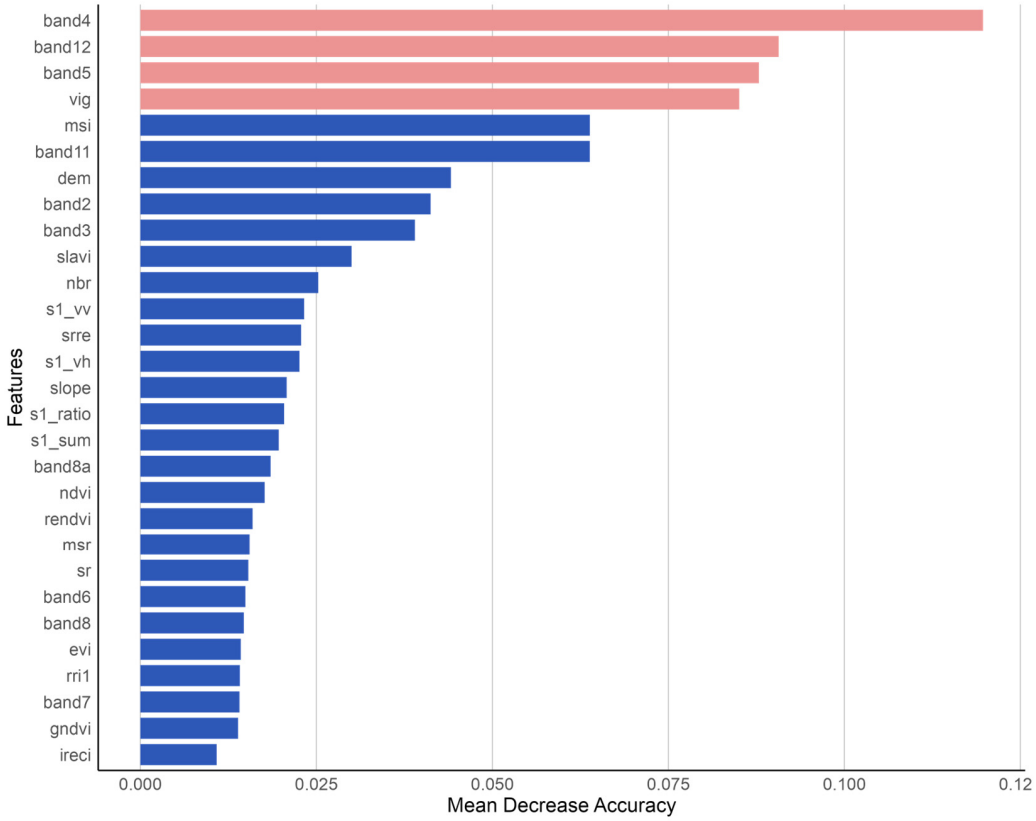

Figure 7. The mean decrease accuracy and ranking of the 29 variables for the ecotone upscaling model. Pink bars indicate the four most important variables in the model.

3.3. Temporal Dynamic Analysis of Ecotones

By applying the upscaling model to the satellite images of 2017 and 2023, the landscape pattern maps of ecotones in these two years were obtained (Figure 8) and the area of different land use types was calculated, with the "Others" category including grassland, water, road and other classes except forest and ecotone. Overall, the area of the ecotones increased by 0.287 km^2 in these six years (Table 7).

Table 7. The area of different land use types in 2017 and 2023 (km^2).

Year	Ecotones	Forests	Others
2017	26.2098	133.5169	11.2733
2023	26.4968	131.5166	12.9866

We also calculated a transition matrix describing the land cover change in the 2017–2023 period (Table 8). The results indicate that changes in ecotones and other land use types were substantial, whereas forests remained relatively stable. Additionally, the expansion of ecotone areas primarily originated from non-forest land uses.

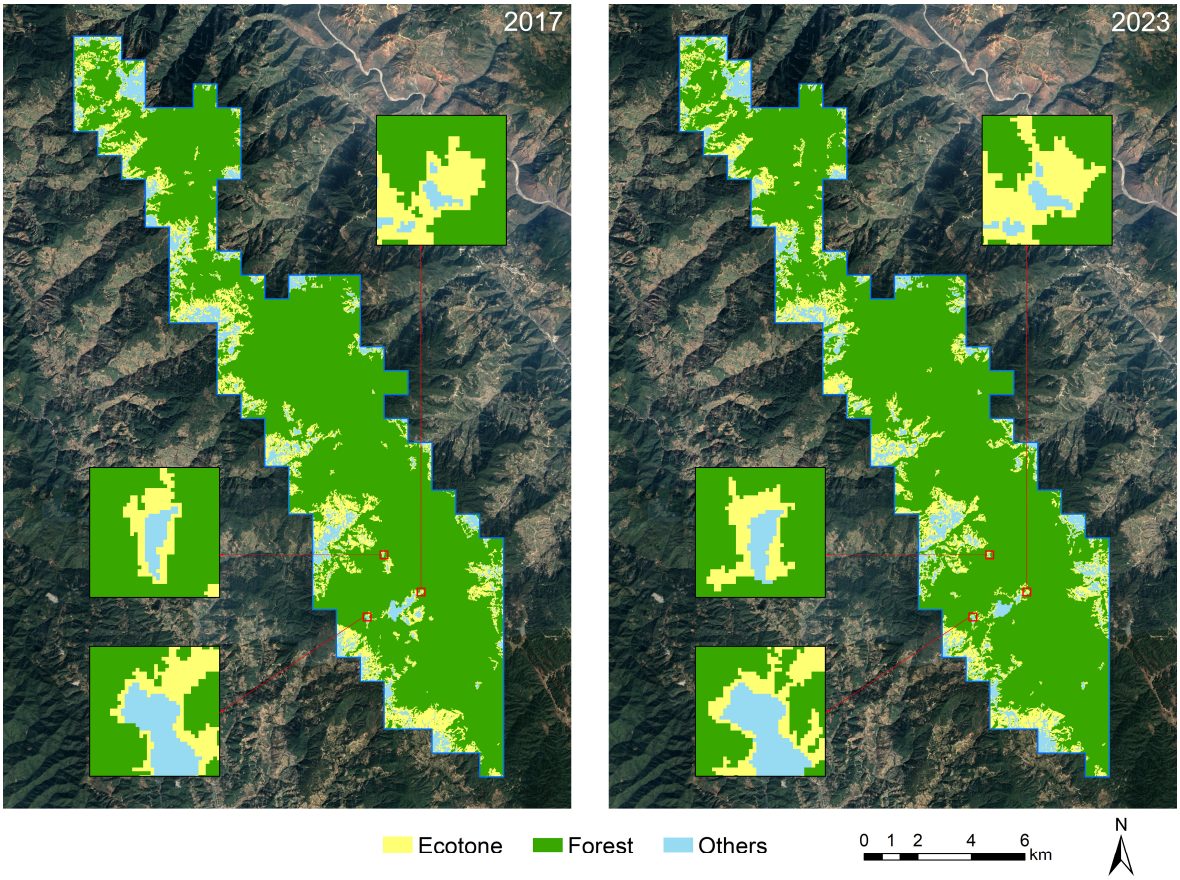

Figure 8. The landscape pattern maps of ecotones in 2017 and 2023.

Table 8. Land cover change transition matrix for the whole region (in km^2).

2017	2023		
	Ecotones	**Forests**	**Others**
Ecotones	17.561 (67%) [1]	4.8574 (18.5%)	3.7914 (14.5%)
Forests	7.1035 (5.3%)	126.0671 (94.4%)	0.3463 (0.3%)
Others	1.8323 (16.3%)	0.5921 (5.3%)	8.8489 (78.5%)

[1] The values in parentheses represent the proportions of land use types transformed from 2017 to 2023.

The quantitative analysis results of landscape fragmentation (Table 9) show that the PD, ED, and FI all decreased, while the MPA increased, indicating that the degree of landscape fragmentation of forests decreased. However, fragmentation increased in the ecotones and other categories.

Table 9. A series of landscape metrics used to quantify landscape fragmentation at a large scale.

Metrics	Forest		Ecotones		Others	
	2017	**2023**	**2017**	**2023**	**2017**	**2023**
PD	4.83	4.67	3.82	4.47	5.53	6.42
ED	57.16	56.63	86.26	90.46	33.17	39.56
MPA	16.16	16.46	4.01	3.27	1.19	1.18
FI	26.05	25.92	31.37	32.82	13.3	15.72

4. Discussion

Since ecotones are considered sensitive indicators of climate and land use change (including forest fragmentation), accurately tracking their dynamics is important [55,56]. With the increased spatial and temporal resolution of remote sensing data, extracting and tracking ecotones at large scales has become available in principle [57]. However, difficulties exist in using the relatively coarse remote sensing data for extracting fine-scale ecotones. Our results show that combining UAV-based and satellite data can fill this surface analysis and monitoring gap. The proposed integration leverages the high-resolution capabilities of drones for detailed observations and the extensive coverage of satellites, thereby enhancing the overall accuracy and scope of environmental assessments focusing on ecotones.

4.1. Delineating Ecotones on the UAV Scale

The heterogeneous character of any landscape (mosaic) significantly influences many ecological processes [58,59]. Figure 5 shows the presence of ecotones formed a more complicated landscape pattern. Despite their crucial role in enhancing landscape heterogeneity, ecotones are often ignored in traditional landscape analyses. Conventional studies utilizing remote sensing image data have identified transition zones and landscape boundaries on a larger scale [60]. However, some gradual transition zones between different landscape units or patches are also easily overlooked due to the limitations in the resolution of satellite imagery.

Utilizing Unmanned Aerial Systems (UAS) for photography offers a higher resolution alternative that provides a potential advantage over traditional satellite remote sensing methods in studying ecotones at regional and fine scales. This method enables comprehensive data acquisition on a regional scale, facilitating landscape pattern analysis without needing multiple field investigations, thereby offering significant reductions in time and labor. Furthermore, UAV-LiDAR data have proven previous studies for delineating transitions in forest and vegetation, particularly in highlighting height variations among plant communities. Such precise data are crucial for accurately mapping forest-grassland ecotones, offering advantages over traditional airborne and spaceborne LiDAR technologies in terms of flexibility, cost, and data density [61]. As a newly emerging and low-cost active remote sensing technology, UAV-LiDAR can characterize the vertical structure of forest ecosystems at a fine spatial resolution [62], even for the attributes of individual trees [63].

From an applied perspective, our methodology employs high-resolution UAV-acquired orthoimage and LiDAR data to achieve highly accurate ecotone delineation, revealing discrete ecological gradients and previously undetected transitional patterns. The resulting high-resolution land cover map incorporating these ecotonal features provides new insights into ecosystem dynamics, delivering critical information for evidence-based conservation planning in ecologically sensitive regions. Notably, our findings demonstrate how spatially explicit data enables optimized intervention strategies through precise identification of ecological transition zones, which may significantly improve cost-effectiveness in long-term landscape management. While existing studies have successfully applied this technology to small-scale feature extraction (e.g., individual trees and linear vegetation structures [34,64]), our research establishes a novel framework for the 3D characterization of complex ecotonal systems. Specifically, the developed approach for forest-grassland ecotone identification offers a three-dimensional analytical perspective that enhances environmental decision-making processes and resource allocation efficiency. Furthermore, the precisely mapped ecotones could serve as reference data for upscaling methodologies, facilitating integration with coarse-resolution satellite datasets to enable large-area ecotone monitoring while maintaining classification accuracy. This methodological advancement not only improves

ecological management strategies but also provides new opportunities for understanding landscape-level ecological processes.

4.2. Upscaling from the UAV Scale to the Sentinel Scale

Our results demonstrate that the combination of UAV and satellite imagery, particularly through an upscaling model constructed from this integration, accurately delineated forest-grassland ecotones with a kappa coefficient of 0.78 (Table 6). This indicates a robust capability to monitor their dynamics effectively. Direct spatial correlation between UAV imagery and Sentinel products improved the accuracy by utilizing an overhead canopy perspective, unlike field-based estimates, thereby providing a continuous landscape representation. Our findings furthermore reveal that the accuracy of the ecotone upscaling model was significantly influenced by the choice of input variables, with the 11 most important variables all extracted from Sentinel-2 multispectral data (Figure 7). This suggests that Sentinel-2 data are more suitable than the SAR data from Sentinel-1 for detecting forest-grassland ecotones. Although combining Sentinel-1 with Sentinel-2 data can further improve accuracy, previous studies have shown that optical data is generally ascribed to a higher potential than SAR data [65]. Despite the relatively small contribution, incorporating Sentinel-1 data may still be advantageous, particularly in regions with frequent cloud cover where the availability of high-quality spectral data from Sentinel-2 is constrained. Furthermore, coupling the accessibility and cost-effectiveness of Sentinel-1 data with preprocessing routines can enhance data robustness under challenging observational conditions. Additionally, while grayscale covariance matrix-based image texture features are usually utilized in large-scale ecotone extraction [66,67], their effectiveness diminishes in areas with complex terrain, such as the Ailao Mountain National Nature Reserve, where they tend to decrease classification accuracy. This suggests a need for careful selection and application of texture features based on the specific geographical and ecological characteristics of the study area.

The presented approach is easily transferable to other regions and can be applied to detect different types of small biotopes, such as abandoned land-forest ecotones, agricultural terraces, etc. [23,68]. Categorizing transition zones as distinct land use types within existing land change monitoring frameworks can help evaluate and optimize management zones of existing nature reserves and establish additional protected areas [69–71]. Moreover, our results suggest that upscaling UAV-based reference data to satellite-based earth observation systems offers significant potential for vegetation-related mapping tasks. This approach could enhance applications in tree species classification for forestry, biodiversity assessments, and habitat mapping by supplementing low-resolution satellite images with detailed, high-resolution data [72,73].

We have demonstrated that integrating multi-source remote sensing data facilitates large-scale ecotone detection. By incorporating diverse satellite data types, such as hyperspectral imagery and LiDAR from various platforms, we could further refine the accuracy of ecotone delineation by capturing detailed biochemical and structural vegetation features. Future research should focus on enhancing ecotone detection accuracy by considering the seasonality of vegetation indices and SAR data bands with a high capacity for penetrating structurally dense forest canopies. This could be done by comparing multi-seasonal remote sensing data and integrating ground-based observations to analyze shifts in ecotone boundaries related to phenological changes. Additionally, this study represents an initial exploration to integrate multi-source remote sensing data, with plans to refine and expand our methods as more and longer data series become available in the future.

5. Conclusions

In this study, we propose a semi-automatic workflow to delineate large-scale ecotones which integrates visual delineation using UAV-derived orthoimages and LiDAR data, training of upscaling model using Sentinel-1 and Sentinel-2 data, and application of this model to monitor ecotone dynamics over different years. Integrating structural and spectral information from UAV data enables more precise delineation of fine-scale ecotones and other small biotopes. The upscaling model was highly accurate for all three plots, demonstrating the potential of upscaling UAV reference data to the Sentinel scale to delineate ecotones over large spatial extents. This study confirms the suitability of UAV-based reference data for training satellite-based models, offering a promising alternative to traditional field-acquired data. The advantages of UAV-based data include consistency in perspective with satellite products (top-down) and ease of spatial matching through resampling. Moreover, UAV data generation is relatively efficient, especially across less accessible terrain. The proposed workflow is easily transferable to other regions and facilitates long-term ecotone monitoring, which is important for understanding the impacts of climate change and forest fragmentation on natural ecosystems.

Author Contributions: Conceptualization, Y.M. and Z.Z.; methodology, Y.M.; software, Y.M. and B.W.; validation, Y.M., W.L. (Weihong Liu) and C.Y.; investigation, Y.M., Z.X., X.S. and N.L.; writing—original draft preparation, Y.M.; writing—review and editing, Y.M., H.J.D.B. and W.L. (Wenjun Liu); supervision, Z.Z. and W.L. (Wenjun Liu). All authors have read and agreed to the published version of the manuscript.

Funding: This work was supported by Major Program for Basic Research Project of Yunnan Province (202101BC070002), the National Key Research and Development Program of China (2022YFF1303103), the National Natural Science Foundation of China (32260300), and the Scientific Research Fund Project of Yunnan Education Department and the Graduate Research Innovation Fund Project of Yunnan University (2025Y0076).

Data Availability Statement: The satellite data are available from the GEE platform (https://code.earthengine.google.com/, accessed on 10 March 2024). All the UAV data and other datasets generated during this study are not publicly available due to size constraints but can be provided by the corresponding authors upon reasonable request. The code used in this study is also available from the corresponding authors upon reasonable request.

Acknowledgments: We express our gratitude to the staff of Ailao Mountain National Nature Reserve and Ailao Mountain Ecological Station, Chinese Academy of Sciences, for their assistance in conducting our research. We appreciate the critical and constructive comments and suggestions from the reviewers that helped improve the quality of this manuscript.

Conflicts of Interest: The authors declare no conflicts of interest.

References

1. Clements, F.E. *Research Methods in Ecology*; University Publishing Company: Lincoln, NE, USA, 1905.
2. Fortin, M.-J.; Olson, R.J.; Ferson, S.; Iverson, L.; Hunsaker, C.; Edwards, G.; Levine, D.; Butera, K.; Klemas, V. Issues Related to the Detection of Boundaries. *Landsc. Ecol.* **2000**, *15*, 453–466. [CrossRef]
3. Watkins, R.Z.; Chen, J.; Pickens, J.; Brosofske, K.D. Effects of Forest Roads on Understory Plants in a Managed Hardwood Landscape. *Conserv. Biol.* **2003**, *17*, 411–419. [CrossRef]
4. Yarrow, M.M.; Marín, V.H. Toward Conceptual Cohesiveness: A Historical Analysis of the Theory and Utility of Ecological Boundaries and Transition Zones. *Ecosystems* **2007**, *10*, 462–476. [CrossRef]
5. Hufkens, K.; Scheunders, P.; Ceulemans, R. Ecotones in Vegetation Ecology: Methodologies and Definitions Revisited. *Ecol. Res.* **2009**, *24*, 977–986. [CrossRef]
6. Fahrig, L. Effects of Habitat Fragmentation on Biodiversity. *Annu. Rev. Ecol. Evol. Syst.* **2003**, *34*, 487–515. [CrossRef]
7. Haddad, N.M.; Brudvig, L.A.; Clobert, J.; Davies, K.F.; Gonzalez, A.; Holt, R.D.; Lovejoy, T.E.; Sexton, J.O.; Austin, M.P.; Collins, C.D.; et al. Habitat Fragmentation and Its Lasting Impact on Earth's Ecosystems. *Sci. Adv.* **2015**, *1*, e1500052. [CrossRef]

8. Foster, J.R.; D'Amato, A.W. Montane Forest Ecotones Moved Downslope in Northeastern USA in Spite of Warming between 1984 and 2011. *Glob. Change Biol.* **2015**, *21*, 4497–4507. [CrossRef] [PubMed]
9. Brownstein, G.; Johns, C.; Fletcher, A.; Pritchard, D.; Erskine, P.D. Ecotones as Indicators: Boundary Properties in Wetland-Woodland Transition Zones. *Community Ecol.* **2015**, *16*, 235–243. [CrossRef]
10. Moraes, M.C.P.d.; Mello, K.d.; Toppa, R.H. Protected Areas and Agricultural Expansion: Biodiversity Conservation versus Economic Growth in the Southeast of Brazil. *J. Environ. Manag.* **2017**, *188*, 73–84. [CrossRef]
11. Fisher, P.; Arnot, C.; Wadsworth, R.; Wellens, J. Detecting Change in Vague Interpretations of Landscapes. *Ecol. Inform.* **2006**, *1*, 163–178. [CrossRef]
12. Zhang, J.; Wei, J.; Chen, Q.G. Mapping the Farming-Pastoral Ecotones in China. *J. Mt. Sci.* **2009**, *6*, 78–87. [CrossRef]
13. Cardoso, A.W.; Oliveras, I.; Abernethy, K.A.; Jeffery, K.J.; Glover, S.; Lehmann, D.; Edzang Ndong, J.; White, L.J.T.; Bond, W.J.; Malhi, Y. A Distinct Ecotonal Tree Community Exists at Central African Forest–Savanna Transitions. *J. Ecol.* **2021**, *109*, 1170–1183. [CrossRef]
14. Ranson, K.J.; Montesano, P.M.; Nelson, R. Object-Based Mapping of the Circumpolar Taiga–Tundra Ecotone with MODIS Tree Cover. *Remote Sens. Environ.* **2011**, *115*, 3670–3680. [CrossRef]
15. Guo, W.K.; Rees, W.G. Altitudinal Forest-Tundra Ecotone Categorization Using Texture-Based Classification. *Remote Sens. Environ.* **2019**, *232*, 111312. [CrossRef]
16. Kharuk, V.I.; Im, S.T.; Dvinskaya, M.L. Forest–Tundra Ecotone Response to Climate Change in the Western Sayan Mountains, Siberia. *Scand. J. For. Res.* **2010**, *25*, 224–233. [CrossRef]
17. Tan, J.B.; Chen, M.Q.; Ao, C.; Zhao, G.; Lei, G.B.; Tang, Y.; Wang, B.; Li, A.N. Inducing Flooding Index for Vegetation Mapping in Water-Land Ecotone with Sentinel-1 & Sentinel-2 Images: A Case Study in Dongting Lake, China. *Ecol. Indic.* **2022**, *144*, 109448. [CrossRef]
18. Wei, B.C.; Xie, Y.W.; Wang, X.Y.; Jiao, J.Z.; He, S.J.; Bie, Q.; Jia, X.; Xue, X.Y.; Duan, H.M. Land Cover Mapping Based on Time-series MODIS-NDVI Using a Dynamic Time Warping Approach: A Casestudy of the Agricultural Pastoral Ecotone of Northern China. *Land Degrad. Dev.* **2020**, *31*, 1050–1068. [CrossRef]
19. Morley, P.J.; Donoghue, D.N.M.; Chen, J.-C.; Jump, A.S. Quantifying Structural Diversity to Better Estimate Change at Mountain Forest Margins. *Remote Sens. Environ.* **2019**, *223*, 291–306. [CrossRef]
20. Hoechstetter, S.; Thinh, N.; Walz, U. 3D-Indices for the Analysis of Spatial Patterns of Landscape Structure. *Proc. InterCarto-InterGIS* **2006**, *12*, 108–118.
21. Hill, R.; Granica, K.; Smith, G.; Schardt, M. Representation of an Alpine Treeline Ecotone in SPOT 5 HRG Data. *Remote Sens. Environ.* **2007**, *110*, 458–467. [CrossRef]
22. Hou, W.; Walz, U. Extraction of Small Biotopes and Ecotones from Multi-Temporal RapidEye Data and a High-Resolution Normalized Digital Surface Model. *Int. J. Remote Sens.* **2014**, *35*, 7245–7262. [CrossRef]
23. Wang, B.; Sun, H.; Cracknell, A.P.; Deng, Y.; Li, Q.; Lin, L.X.; Xu, Q.; Ma, Y.X.; Wang, W.L.; Zhang, Z.M. Detection and Quantification of Forest-Agriculture Ecotones Caused by Returning Farmland to Forest Program Using Unmanned Aircraft Imagery. *Diversity* **2022**, *14*, 406. [CrossRef]
24. Ørka, H.O.; Wulder, M.A.; Gobakken, T.; Næsset, E. Subalpine Zone Delineation Using LiDAR and Landsat Imagery. *Remote Sens. Environ.* **2012**, *119*, 11–20. [CrossRef]
25. Coops, N.C.; Morsdorf, F.; Schaepman, M.E.; Zimmermann, N.E. Characterization of an Alpine Tree Line Using Airborne LiDAR Data and Physiological Modeling. *Glob. Change Biol.* **2013**, *19*, 3808–3821. [CrossRef] [PubMed]
26. Shahbazi, M.; Théau, J.; Ménard, P. Recent Applications of Unmanned Aerial Imagery in Natural Resource Management. *GISci. Remote Sens.* **2014**, *51*, 339–365. [CrossRef]
27. Gonzalez Musso, R.F.; Oddi, F.J.; Goldenberg, M.G.; Garibaldi, L.A. Applying Unmanned Aerial Vehicles (UAVs) to Map Shrubland Structural Attributes in Northern Patagonia, Argentina. *Can. J. For. Res.* **2020**, *50*, 615–623. [CrossRef]
28. Yang, X.; Yao, Z.L.; Wang, B.; Wen, H.D.; Deng, Y.; Cao, M.; Zhang, Z.M.; Tan, Z.H.; Lin, L.X. Driving Effects of Forest Stand Structure of a Subtropical Evergreen Broad-Leaved Forest on Species Composition Variation: From Local to Regional Scales. *Biodivers. Sci.* **2023**, *31*, 22139. [CrossRef]
29. Wu, C.S.; Sha, L.Q.; Zhang, Y.P. Effect of Litter on Soil Respiration and Its Temperature Sensitivity in a Montane Evergreen Broad-Leaved Forest in Ailao Mountains, Yunnan. *J. Northeast. For. Univ.* **2012**, *40*, 37–40. [CrossRef]
30. Wen, H.D.; Lin, L.X.; Yang, J.; Hu, Y.H.; Cao, M.; Liu, Y.H.; Lu, Z.Y.; Xie, Y.N. Species composition and community structure of a 20 hm2 plot of mid-mountain moist evergreen broad-leaved forest on the Mts. Ailaoshan, Yunnan Province, China. *Chin. J. Plant Ecol.* **2018**, *42*, 419–429. [CrossRef]
31. Torres de Almeida, C.; Gerente, J.; Rodrigo dos Prazeres Campos, J.; Caruso Gomes Junior, F.; Providelo, L.A.; Marchiori, G.; Chen, X. Canopy Height Mapping by Sentinel 1 and 2 Satellite Images, Airborne LiDAR Data, and Machine Learning. *Remote Sens.* **2022**, *14*, 4112. [CrossRef]

32. Nasirzadehdizaji, R.; Balik Sanli, F.; Abdikan, S.; Cakir, Z.; Sekertekin, A.; Ustuner, M. Sensitivity Analysis of Multi-Temporal Sentinel-1 SAR Parameters to Crop Height and Canopy Coverage. *Appl. Sci.* **2019**, *9*, 655. [CrossRef]
33. Hijmans, R.J. Terra: Spatial Data Analysis. 2024. Available online: https://rspatial.github.io/terra (accessed on 23 February 2025).
34. Hou, W.; Walz, U. Enhanced Analysis of Landscape Structure: Inclusion of Transition Zones and Small-Scale Landscape Elements. *Ecol. Indic.* **2013**, *31*, 15–24. [CrossRef]
35. Riihimäki, H.; Luoto, M.; Heiskanen, J. Estimating Fractional Cover of Tundra Vegetation at Multiple Scales Using Unmanned Aerial Systems and Optical Satellite Data. *Remote Sens. Environ.* **2019**, *224*, 119–132. [CrossRef]
36. Hesselbarth, M.H.K.; Sciaini, M.; With, K.A.; Wiegand, K.; Nowosad, J. Landscapemetrics: An Open-Source R Tool to Calculate Landscape Metrics. *Ecography* **2019**, *42*, 1648–1657. [CrossRef]
37. Loke, L.H.L.; Chisholm, R.A.; Todd, P.A. Effects of Habitat Area and Spatial Configuration on Biodiversity in an Experimental Intertidal Community. *Ecology* **2019**, *100*, e02757. [CrossRef] [PubMed]
38. Umaña, M.N.; Mi, X.; Cao, M.; Enquist, B.J.; Hao, Z.; Howe, R.; Iida, Y.; Johnson, D.; Lin, L.; Liu, X.; et al. The Role of Functional Uniqueness and Spatial Aggregation in Explaining Rarity in Trees. *Glob. Ecol. Biogeogr.* **2017**, *26*, 777–786. [CrossRef]
39. Nams, V.O. Shape of Patch Edges Affects Edge Permeability for Meadow Voles. *Ecol. Appl.* **2012**, *22*, 1827–1837. [CrossRef] [PubMed]
40. Altman, N.S. An Introduction to Kernel and Nearest-Neighbor Nonparametric Regression. *Am. Stat.* **1992**, *46*, 175–185. [CrossRef]
41. Maselli, F.; Chirici, G.; Bottai, L.; Corona, P.; Marchetti, M. Estimation of Mediterranean Forest Attributes by the Application of k-NN Procedures to Multitemporal Landsat ETM+ Images. *Int. J. Remote Sens.* **2005**, *26*, 3781–3796. [CrossRef]
42. Belgiu, M.; Drăguţ, L. Random Forest in Remote Sensing: A Review of Applications and Future Directions. *ISPRS J. Photogramm. Remote Sens.* **2016**, *114*, 24–31. [CrossRef]
43. Cortes, C.; Vapnik, V. Support-Vector Networks. *Mach. Learn.* **1995**, *20*, 273–297. [CrossRef]
44. Huang, C.; Davis, L.S.; Townshend, J.R.G. An Assessment of Support Vector Machines for Land Cover Classification. *Int. J. Remote Sens.* **2002**, *23*, 725–749. [CrossRef]
45. Foody, G.M.; Mathur, A. A Relative Evaluation of Multiclass Image Classification by Support Vector Machines. *IEEE Trans. Geosci. Remote Sens.* **2004**, *42*, 1335–1343. [CrossRef]
46. Qian, Y.G.; Zhou, W.Q.; Yan, J.L.; Li, W.F.; Han, L.J. Comparing Machine Learning Classifiers for Object-Based Land Cover Classification Using Very High Resolution Imagery. *Remote Sens.* **2015**, *7*, 153–168. [CrossRef]
47. Zhang, B.H.; Zhang, L.; Xie, D.; Yin, X.L.; Liu, C.J.; Liu, G. Application of Synthetic NDVI Time Series Blended from Landsat and MODIS Data for Grassland Biomass Estimation. *Remote Sens.* **2016**, *8*, 10. [CrossRef]
48. Mason, L.; Baxter, J.; Bartlett, P.; Frean, M. Boosting Algorithms as Gradient Descent. In *Proceedings of the Advances in Neural Information Processing Systems*; MIT Press: Cambridge, MA, USA, 1999; Volume 12.
49. Puertas, O.L.; Brenning, A.; Meza, F.J. Balancing Misclassification Errors of Land Cover Classification Maps Using Support Vector Machines and Landsat Imagery in the Maipo River Basin (Central Chile, 1975–2010). *Remote Sens. Environ.* **2013**, *137*, 112–123. [CrossRef]
50. Alexander, C.; Tansey, K.; Kaduk, J.; Holland, D.; Tate, N.J. Backscatter Coefficient as an Attribute for the Classification of Full-Waveform Airborne Laser Scanning Data in Urban Areas. *ISPRS-J. Photogramm. Remote Sens.* **2010**, *65*, 423–432. [CrossRef]
51. Pedregosa, F.; Varoquaux, G.; Gramfort, A.; Michel, V.; Thirion, B.; Grisel, O.; Blondel, M.; Prettenhofer, P.; Weiss, R.; Dubourg, V.; et al. Scikit-Learn: Machine Learning in Python. *J. Mach. Learn. Res.* **2011**, *12*, 2825–2830.
52. Phiri, D.; Simwanda, M.; Salekin, S.; Nyirenda, V.; Murayama, Y.; Ranagalage, M. Sentinel-2 Data for Land Cover/Use Mapping: A Review. *Remote Sens.* **2020**, *12*, 2291. [CrossRef]
53. Ma, J.; Li, J.W.; Wu, W.B.; Liu, J.J. Global Forest Fragmentation Change from 2000 to 2020. *Nat. Commun.* **2023**, *14*, 3752. [CrossRef] [PubMed]
54. Forman, R.T.T. *Land Mosaics: The Ecology of Landscapes and Regions*; Cambridge University Press: Cambridge, MA, USA, 1995.
55. Kupfer, J.A.; Cairns, D.M. The Suitability of Montane Ecotones as Indicators of Global Climatic Change. *Prog. Phys. Geogr.* **1996**, *20*, 253–272. [CrossRef]
56. Walker, S.; Wilson, J.B.; Steel, J.B.; Rapson, G.L.; Smith, B.; King, W.M.; Cottam, Y.H. Properties of Ecotones: Evidence from Five Ecotones Objectively Determined from a Coastal Vegetation Gradient. *J. Veg. Sci.* **2003**, *14*, 579–590. [CrossRef]
57. Nguyen, T.-A.; Kellenberger, B.; Tuia, D. Mapping Forest in the Swiss Alps Treeline Ecotone with Explainable Deep Learning. *Remote Sens. Environ.* **2022**, *281*, 113217. [CrossRef]
58. Hansen, A.J.; Di Castri, F. (Eds.) *Landscape Boundaries*; Ecological Studies; Springer: New York, NY, USA, 1992; Volume 92, ISBN 978-1-4612-7677-7.
59. Farina, A. Scaling Patterns and Processes across Landscapes. In *Principles and Methods in Landscape Ecology*; Farina, A., Ed.; Springer: Dordrecht, The Netherlands, 1998; pp. 35–49, ISBN 978-94-015-8984-0.

60. Ranson, K.J.; Sun, G.; Kharuk, V.I.; Kovacs, K. Assessing Tundra–Taiga Boundary with Multi-Sensor Satellite Data. *Remote Sens. Environ.* **2004**, *93*, 283–295. [CrossRef]
61. Nelson, R.; Margolis, H.; Montesano, P.; Sun, G.; Cook, B.; Corp, L.; Andersen, H.-E.; deJong, B.; Pellat, F.P.; Fickel, T.; et al. Lidar-Based Estimates of Aboveground Biomass in the Continental US and Mexico Using Ground, Airborne, and Satellite Observations. *Remote Sens. Environ.* **2017**, *188*, 127–140. [CrossRef]
62. Guo, Q.H.; Su, Y.J.; Hu, T.Y.; Zhao, X.Q.; Wu, F.F.; Li, Y.M.; Liu, J.; Chen, L.H.; Xu, G.C.; Lin, G.H.; et al. An Integrated UAV-Borne Lidar System for 3D Habitat Mapping in Three Forest Ecosystems across China. *Int. J. Remote Sens.* **2017**, *38*, 2954–2972. [CrossRef]
63. Qin, H.M.; Zhou, W.Q.; Yao, Y.; Wang, W.M. Individual Tree Segmentation and Tree Species Classification in Subtropical Broadleaf Forests Using UAV-Based LiDAR, Hyperspectral, and Ultrahigh-Resolution RGB Data. *Remote Sens. Environ.* **2022**, *280*, 113143. [CrossRef]
64. Lin, Y.; Yao, S.B. Impact of the Sloping Land Conversion Program on Rural Household Income: An Integrated Estimation. *Land Use Policy* **2014**, *40*, 56–63. [CrossRef]
65. Fassnacht, F.E.; Latifi, H.; Stereńczak, K.; Modzelewska, A.; Lefsky, M.; Waser, L.T.; Straub, C.; Ghosh, A. Review of Studies on Tree Species Classification from Remotely Sensed Data. *Remote Sens. Environ.* **2016**, *186*, 64–87. [CrossRef]
66. Khatami, R.; Mountrakis, G.; Stehman, S.V. A Meta-Analysis of Remote Sensing Research on Supervised Pixel-Based Land-Cover Image Classification Processes: General Guidelines for Practitioners and Future Research. *Remote Sens. Environ.* **2016**, *177*, 89–100. [CrossRef]
67. Rösch, M.; Sonnenschein, R.; Buchelt, S.; Ullmann, T. Comparing PlanetScope and Sentinel-2 Imagery for Mapping Mountain Pines in the Sarntal Alps, Italy. *Remote Sens.* **2022**, *14*, 3190. [CrossRef]
68. Diaz-Varela, R.A.; Zarco-Tejada, P.J.; Angileri, V.; Loudjani, P. Automatic identification of agricultural terraces through object-oriented analysis of very high resolution DSMs and multispectral imagery obtained from an unmanned aerial vehicle. *J. Environ. Manag.* **2014**, *134*, 117–126. [CrossRef]
69. Hou, W.; Neubert, M.; Walz, U. A Simplified Econet Model for Mapping and Evaluating Structural Connectivity with Particular Attention of Ecotones, Small Habitats, and Barriers. *Landsc. Urban Plan.* **2017**, *160*, 28–37. [CrossRef]
70. Keeley, A.T.H.; Beier, P.; Jenness, J.S. Connectivity Metrics for Conservation Planning and Monitoring. *Biol. Conserv.* **2021**, *255*, 109008. [CrossRef]
71. Lu, Y.; Huang, D.; Liu, Y.; Zhang, Y.; Jing, Y.; Chen, H.; Zhang, Z.; Liu, Y. Exploring the Optimization and Management Methods of Ecological Networks Based on the Cluster Mode: A Case Study of Wuhan Metropolis, China. *Land Use Policy* **2024**, *137*, 107021. [CrossRef]
72. Immitzer, M.; Böck, S.; Einzmann, K.; Vuolo, F.; Pinnel, N.; Wallner, A.; Atzberger, C. Fractional Cover Mapping of Spruce and Pine at 1 Ha Resolution Combining Very High and Medium Spatial Resolution Satellite Imagery. *Remote Sens. Environ.* **2018**, *204*, 690–703. [CrossRef]
73. Leitão, P.J.; Schwieder, M.; Pötzschner, F.; Pinto, J.R.R.; Teixeira, A.M.C.; Pedroni, F.; Sanchez, M.; Rogass, C.; van der Linden, S.; Bustamante, M.M.C.; et al. From Sample to Pixel: Multi-scale Remote Sensing Data for Upscaling Aboveground Carbon Data in Heterogeneous Landscapes. *Ecosphere* **2018**, *9*, e02298. [CrossRef]